Pulsed surface acoustic waves accelerate wound healing and reveal new parameter limits for cell stimulation in vitro

Kathrin Baumgartner, Paul Täufer, Michelle Lienhart, Rainer Lienhart, Christoph Westerhausen

Angaben zur Veröffentlichung / Publication details:

Baumgartner, Kathrin, Paul Täufer, Michelle Lienhart, Rainer Lienhart, and Christoph Westerhausen. 2024. "Pulsed surface acoustic waves accelerate wound healing and reveal new parameter limits for cell stimulation in vitro." Journal of Physics D: Applied Physics 57 (15): 155401. https://doi.org/10.1088/1361-6463/ad18fa.

Pulsed surface acoustic waves accelerate wound healing and reveal new parameter limits for cell stimulation in vitro

Kathrin Baumgartner[1,2,3], Paul Täufer[2], Michelle Lienhart[2,4], Rainer Lienhart[5] and Christoph Westerhausen[1,2,3,6*]

[1] Institute of Theoretical Medicine, Physiology, University of Augsburg, 86159 Augsburg, Germany
[2] Institute of Physics, Experimental Physics I, University of Augsburg, 86159 Augsburg, Germany
[3] Center for NanoScience (CeNS), Ludwig-Maximilians-Universität Munich, 80799 Munich, Germany
[4] Walter Schottky Institute, School of Natural Sciences, Technische Universität München, 85748 Garching, Germany
[5] Institute of Computer Science, Machine Learning and Computer Vision, University of Augsburg, 86159 Augsburg, Germany
[6] Augsburg Center for Innovative Technologies (ACIT), 86159 Augsburg, Germany
*Corresponding author: christoph.westerhausen@gmail.com

ABSTRACT

The use of surface acoustic waves (SAW) in cell biology has gained high attention in the past years. Previous works show that SAW treatment of artificial wounds in vitro can accelerate wound healing by up to +135 %. However, little is known about the mechanobiourlogy behind these effects, and a stimulation has only been proven for continuous SAW signals so far. We here show that the stimulation efficacy observed in previous studies is preserved for pulsed stimuli applied to MDCK-II cells in wound healing assays on SAW chips at a resonance frequency f_{SAW} = 160 MHz. Moreover, for a reproducible and reliable image analysis, we present the SegFormer-based deep learning algorithm *Neural Cell Edge Detector* (NeuCED) for the cell edge segmentation and image binarization, that allows an automated determination of the stimulation efficacy. With these tools, we explore a wider range of applicable SAW intensities up to P_{in} = 21 dBm (128 mW) with a maximum stimulation efficacy of E = 201 %. We show that the order of magnitude of the stimulation effect is reproducible under the variation of SAW signal characteristics power P_{in}, duty cycle D and pulse width τ, while the mean energy over time is constant. Below a distinct pulse duration limit τ = 100 ms, no direct stimulation effect was observed. From a mechanobiological point of view, these findings and time scales might allow to narrow down the potentially triggered cellular mechanisms during the stimulation.

1. INTRODUCTION

The stimulation of cell growth is a key objective for clinical issues like surgery recovery, chronic wounds, and bone fractures. One of the therapeutic methods prescribed in these cases is ultrasound therapy: Especially low-intensity treatments up to P = 100 mW/cm^2 have been proven to have beneficial effects [1,2]. In physiotherapy, low-frequency, low intensity and/or pulsed ultrasound signals can be used to target possible non-thermal mechanisms in tissue healing [1]. Tajali et al. (2012) concluded that low-intensity pulsed ultrasound can stimulate the radiographic bone healing in fresh fractures [3]. The same type of ultrasound treatment in combination with cryotherapy improved the rehabilitation of patients after total knee replacement surgery [4]. Furthermore, consistent beneficial effects on the healing process of chronic wounds have been observed in patients treated with noncontact low-frequency ultrasound [5], while wound healing in female rats was stimulated by low-intensity pulsed ultrasound signals [6].

In vitro studies can help to explore new stimulation methods and to understand the biomechanics of cell stimulation [7]. A powerful tool to apply or mimic the application of ultrasound for adherent

cultured cells are surface acoustic waves (SAW). The generation of surface acoustic waves on a chip for the stimulation, manipulation and non-invasive analysis of cells has become an established method in cell biology over the past years [8]. Previous studies show that neurite outgrowth of neuroblastoma cells and of primary neurons can be guided by acoustically modulated standing SAW in microchannels [9,10]. In the field of stimulation, Stamp et al. showed that travelling surface acoustic waves at about f_{SAW} = 160 MHz can accelerate SaOs-2 cell growth in wound healing assays by up to +17 % [11]. Another cell line suitable for wound healing assays, that is widely used as model for epithelial studies, are MDCK cells [12]. In 2020, Brugger et al. identified an optimal stimulation range between P_{in} = 6 to 12 dBm (4 to 16 mW) for MDCK-II cells, where wound healing was significantly accelerated by even up to +135 % [13]. In these studies, cell proliferation was not enhanced by SAW, so that the stimulation effect was explained by an accelerated cell migration into the wound. However, the cellular mechanisms that respond to SAW stimulation and promote the migration of cells remain unclear. In the works listed above, wound healing stimulation was only quantified for continuous SAW signals under variation of the intensity, whereas other signal types and their parameters, like SAW pulses, were not yet studied. Furthermore, the treatment of wounds with continuous high-power signals induces high temperatures in the sample, reduced cell viability and did not evoke a stimulation effect in previous works [13]. An understanding of the effects of different SAW signals on the wound healing behavior could help unraveling the underlying mechanisms of SAW stimulation. In this context, Ambattu and Yeo also recently stated that understanding the mechanotransduction mechanisms could advance the SAW stimulation method in the clinical field [14]. Although in vivo systems are more complex than in vitro 2D wound healing models, an explanation of the stimulation effect in vitro could yield essential information on the underlying cellular mechanisms triggered by acoustic stimulation in general.

We here choose a phenomenological approach to this issue and study the limits of applicable SAW intensities, duty cycles and pulse widths of wound healing stimulation in vitro. With this approach, we aim to close the gaps in our understanding of cellular behaviour under stimulation with different SAW signals stated above. Also, we want to overcome the power limit of SAW stimulation and answer the exciting question if a higher maximal power can stimulate stronger if the heat input problem of high-power signals does not appear. Analogous to previous works, where the so far highest SAW-induced stimulation effect was observed, we cultivate MDCK-II cells in wound healing assays using culture inserts on a SAW chip. The exclusion of cells by an elastomeric barrier for wound healing studies is a standardized method to realize 2D cell migration assays [15]. It also has some advantages over cell removal methods like scratch assays by causing less damage to the cell monolayer and increasing the reproducibility of the gap size [16]. For a faster and more reliable image analysis of these wound healing assays, we employ a deep learning- algorithm (NeuCED: **Neu**ral **C**ell **E**dge **D**etector) based on SegFormer [18]. The algorithm detects wound edges in phase contrast scans and converts them to binary images for an automatic determination of the healing velocity. In contrast to previous works, we here stimulate wound healing assays with pulsed instead of continuous SAW signals. Hereby, we will answer the following questions: **1) Can we maximize the stimulation effect with pulsed signals at higher SAW powers compared to previous studies? 2) What is the minimum necessary pulse width of the SAW to stimulate wound healing assays?** Based on our results, we then discuss the cells' viscoelasticity and time scales of mechanotransduction processes involved in acoustic cell stimulation as possible key drivers of the stimulation mechanism.

2. RESULTS

In the following, we present the results of pulsed SAW stimulation of wound healing assays under variation of the SAW power P_{in}, duty cycle D and pulse width τ. We first identify the here employed

SAW signal characteristics in the experimental setup. Second, we present the SegFormer-based deep-learning algorithm NeuCED (**Neu**ral **C**ell **E**dge **D**etector) for an automated image segmentation and determine the stimulation efficacy E of an exemplary wound healing assay stimulated at a high SAW power P_{in} = 21 dBm, D = 10 %, showing that high SAW powers can lead to high stimulation efficacies E = 201 %. Third, we observe that the stimulation effect is conserved under SAW power variation P_{in} within the here employed range as long as the mean energy $\bar{E}_p$ of the pulse remains constant. However, a further variation of the pulse width τ reveals that significant stimulation effects can only be observed for pulse widths $\tau \geq 100$ ms.

All wound healing assays are performed on $LiNbO_3$ chips with a resonance frequency f_{SAW} = 160 MHz. For a detailed description of the materials and methods, see section 5 (Materials and Methods). The experimental design and dimensions of the interdigitated transducers (IDT) with a periodicity of Δx = 25 µm are shown in Figure 1a-b. As a barrier for cell exclusion, we use Ibidi® culture inserts, creating well-defined gaps at a distance $x \approx 50$ µm parallel to the IDT (Figure 1b).

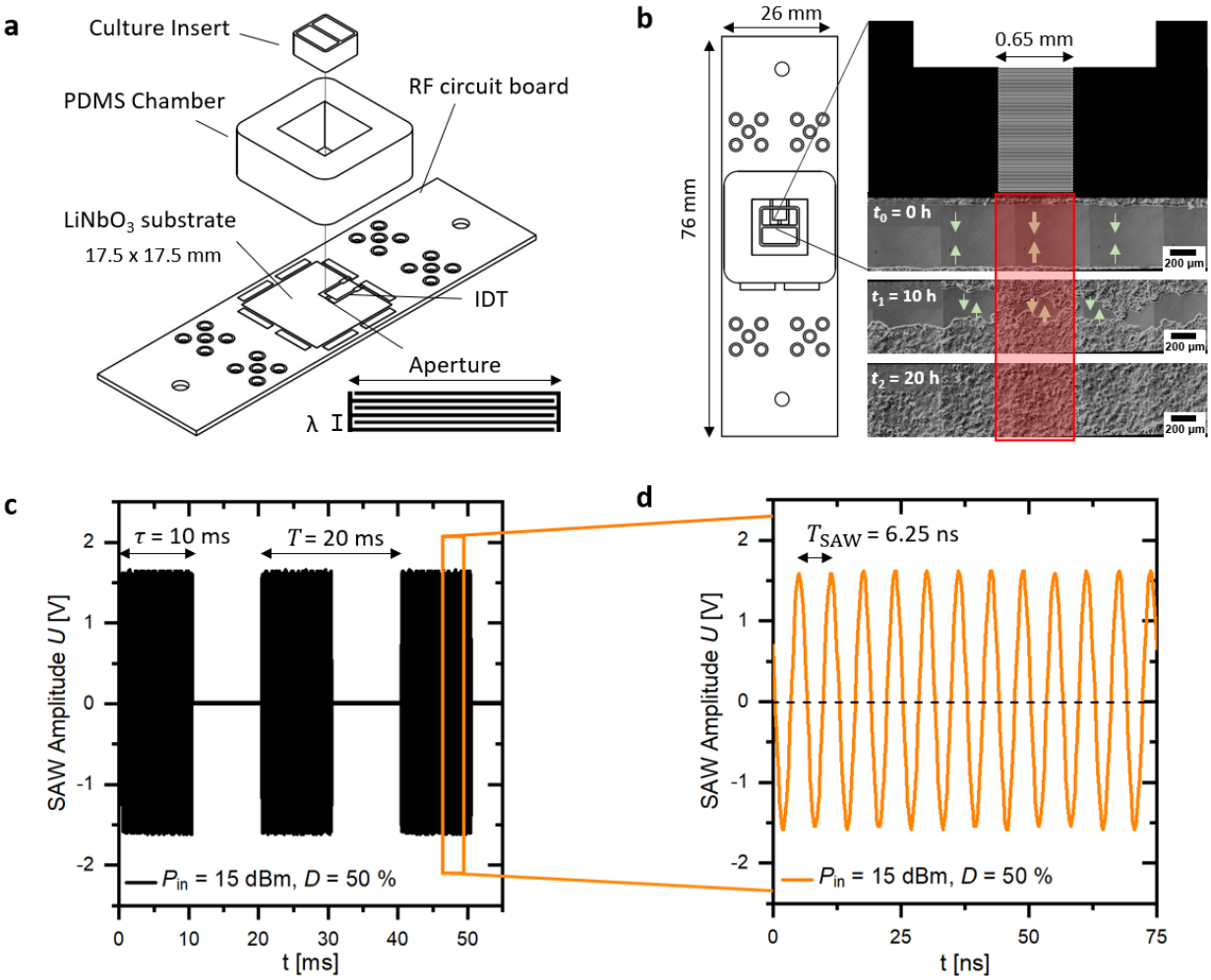

***Figure 1** - Experimental setup and characteristics of the employed pulsed SAW signals. a) Exploded view of the wound healing assay setup on a SAW chip, b) top view with close-up scheme of the IDT and phase contrast images of the artificial wound, where red marks the sound path of the wave, c) oscilloscope records of an exemplary SAW signal at P_{in} = 15 dBm, D = 50 %, d) enlarged view of the oscilloscope signal, where the SAW period T_{SAW} is visible.*

The red rectangle in Fig 1b marks the sound path in front of the aperture, where the SAW signal is generated. We monitor the wound healing process over at least t = 20 h until complete wound closure. Exemplary phase contrast images of the healing process of a SAW-stimulated wound can be seen in

Figure 1b. The oscilloscope records in Figure 1c-d demonstrate the characteristics of the SAW signals used for the wound healing stimulation, where Fig 1c displays an exemplary signal with the parameters P_{in} = 15 dBm, D = 50 % and τ = 10 ms. The duty cycle D of the pulse is defined as:

$$D = \frac{\tau}{T} * 100\,\% \ , \tag{1}$$

where T is the period of the pulse and τ the pulse width. Figure 1d displays a closer view of the signal, so that the period T_{SAW} = 6.25 ns of the SAW becomes visible. We obtain the resonance frequency f_{SAW} = 160 MHz via the relation:

$$f_{SAW} = \frac{1}{T_{SAW}} = \frac{c_{SAW}}{\lambda_{SAW}} \ , \tag{2}$$

where c_{SAW} = 3997 m/s is the sound velocity of a wave propagating on $LiNbO_3$ [17].

The wavelength λ_{SAW} = 25 µm is set by the periodicity of the IDT structure and is roughly in the order of magnitude of a cell. The wavelength also determines the 1/e decay length $L_x^{1/e}$ of the SAW along the propagation direction x: $L_x^{1/e} = 12.5\,\lambda_{SAW} = 331$ µm [18]. At the beginning of the wound healing process, the wound distance is $\Delta x \approx 500$ µm. Consequently, the upper cell front migrates within the decay length $L_x^{1/e}$ during the whole closing process and all cells in the aperture region are under SAW influence during the whole experiment.

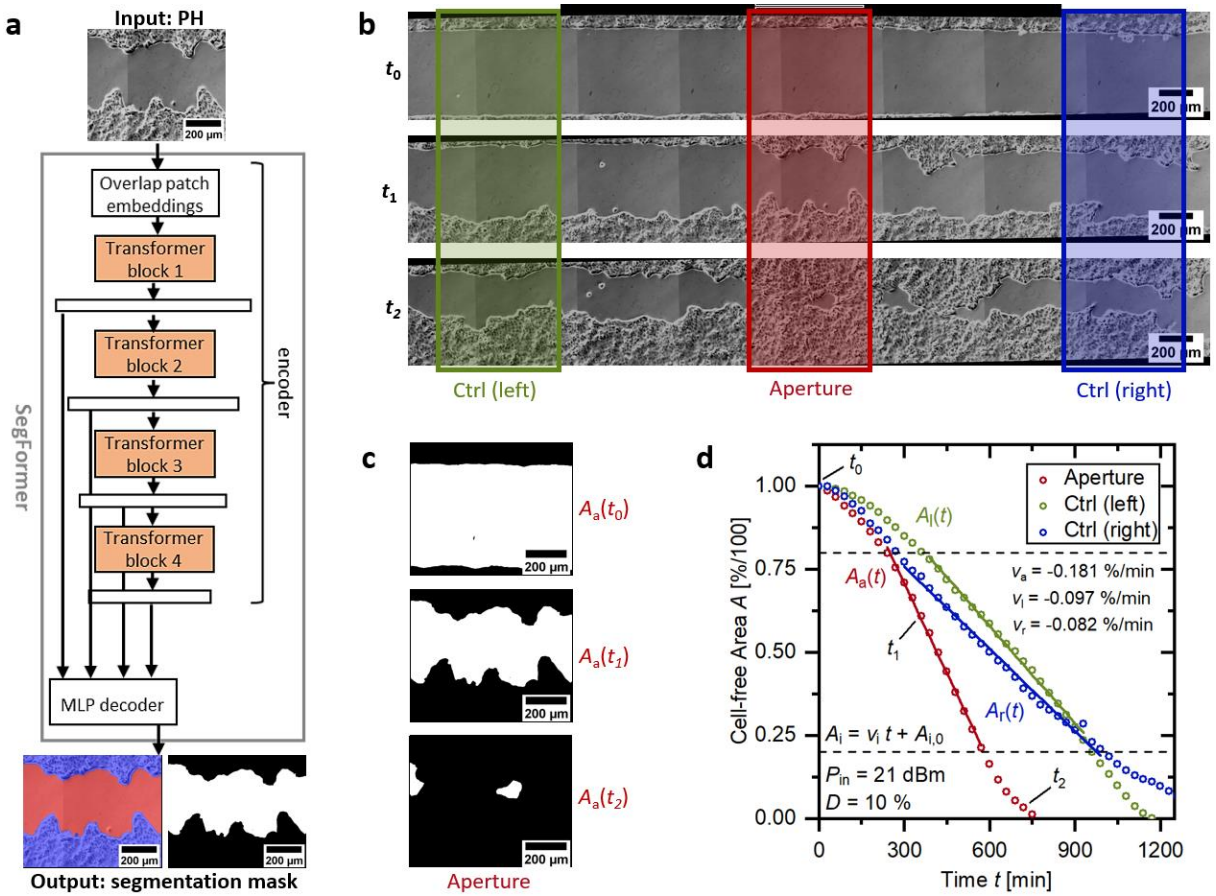

algorithm NeuCED used for automated segmentation of the PH images, b) PH scans at three different time steps t_0 = 0 h, t_1 = 6 h and t_2 = 12 h during the closing process of the wound showing the three regions of interest (aperture and two control regions), c) binarized images of the aperture region at the exemplary time steps, d) exemplary graph of the wound healing processes of the three regions in the sample showing a visible stimulation effect, where the index i in $A_i(t)$ stands for aperture (a), control left (l) or control right (r).

In Figure **2**, we depict an exemplary wound healing analysis under stimulation of a SAW at P_{in} = 21 dBm (128 mW) and D = 10 %. From the phase contrast scans of the wound (Fig 2b), we analyze three regions of interest: the aperture region (red) and two control regions (green and blue) on the edges of the IDT. Only the cells in the aperture region (sound path) are SAW-stimulated, while the other two regions serve as internal controls without SAW influence. A comparison of the wound healing velocity of the regions yields the stimulation efficacy of the sample. However, the determination of the velocity in each region requires the detection of the wound edges. In previous works, these edges were marked manually with the software *ImageJ* [11,13]. To substitute this time-consuming method and to enhance reproducibility, we exploited a SegFormer-based deep-learning segmentation algorithm [18] and integrated it into an automated cell edge detection tool, the Neural Cell Edge Detector (NeuCED, Fig 2a).

The deep-learning based automated cell edge detector NeuCED is based on SegFormer [19], an efficient, accurate, and robust semantic segmentation framework which unifies Transformers [20–24] with lightweight multilayer perceptron (MLP) decoders. As shown in Fig. 2a, the input of NeuCED is a (grayscale) phase contrast image of the wound. SegFormer consists of two main modules: (1) a hierarchical Transformer encoder to generate high-resolution coarse features and low-resolution fine features; and (2) a lightweight MLP decoder to fuse these multi-level features to produce the final semantic segmentation mask (the output of NeuCED). For a detailed description of the SegFormer architecture see section 5 (Materials and Methods) and Xie et al. [19]. By using SegFormer we here demonstrate a highly accurate and very robust cell segmentation framework with a mean intersection over union performance of mIoU = 98.67 % on the test data set. For detailed information on performance and accuracy see SI, Table 1. As apparent from Fig 2a and 2c, the original phase contrast image is binarized into the cell-free background (white) and the area covered with cells (black). The binarization is accurate even if the transition between two stitched images of the scan is not perfectly uniform.

Fig 2b shows an exemplary wound healing process of a sample treated with a pulsed SAW at P_{in} = 21 dBm and D = 10 % at the time steps t_0 = 0 h, t_1 = 6 h and t_2 = 12 h. The binarized images of the aperture region (red) after segmentation with NeuCED are displayed in Fig 2c. To determine the wound healing velocity, we analyze the reduction of the normalized cell-free area A as a function of time t at a step: Δt = 30 min, which is shown in Fig 2d. The area A = 1.0 is the cell free area in the first frame right after the removal of the culture insert and A = 0 represents a fully closed wound. At the beginning, the cells are not immediately polarized in the migration direction after the culture insert removal and at the end, wound closure can be slowed down by uneven collisions of the cell fronts along the wound. Therefore, we approximate the linear decline of the cell-free area only between A = 0.2 and A = 0.8 using a linear regression model, so that the wound healing velocity v_i of a region of interest is given by the slope:

$$A_i = v_i t + A_{i,0} \tag{3}$$

In the here displayed sample, a clear stimulation effect is visible: $|v_a| > |v_r|$ and $|v_a| > |v_l|$. Moreover, the stimulation already becomes visible from the image sequence of the wound healing in Fig 2a. The final stimulation efficacy E of the sample is determined by:

$$E = \frac{v_a}{\frac{1}{2}(v_r + v_l)}, \tag{4}$$

which yields a final stimulation efficacy of E = 201 % for the sample stimulated at P_{in} = 21 dBm. Brugger et al. observed a mean stimulation efficacy E = 235 $\mp$ 80 % at P_{in} = 9 dBm [13], which is in the same

order of magnitude. This shows that a pulsed SAW stimulation of wound healing assays at high powers can be as effective as a continuous stimulation at moderate powers.

The median stimulation efficacy of all control samples (wound healing assays on SAW chips, but without a SAW signal) is $E_{m,Ctrl}$ = 1.04 (N = 24). In general, it is possible that deviations in the wound healing velocity along the wounds can occur due to uneven distributions or polarization of cells, leading to statistical variations. For the following investigations, we therefore tested at least N = 6 samples per each SAW parameter and applied statistical tests to prove the significance of our results. The median of all SAW-treated samples (independent of the detailed parameter set) with a significant stimulation effect in this study is E_m = 1.54 (N = 24). The median wound healing velocities in the aperture regions of the SAW samples and, respectively, of the control samples are: $\bar{v}_{a,SAW} \approx 0.16$ %/min = 48 µm/h and $\bar{v}_{a,Ctrl} \approx 0.10$ %/min = 30 µm/h for an initial wound width of $\Delta x \approx 500$ µm. In control samples, a complete wound closure was achieved after about $t_m \approx 17$ h.

In the following, we investigate the influence of pulsed SAW signals on wound healing assays at different powers P_{in}. We define the mean energy $\bar{E}_p$ of such a pulsed signal:

$$\bar{E}_p = P_{in} \frac{D}{100\%} = const. \tag{5}$$

The condition $\bar{E}_p = const.$ ensures that there are no temperature effects involved in the power variation experiments. The temperature difference for a sample treated with a pulsed SAW at P_{in}= 21 dBm - the highest power used in this study – does not exceed $\Delta T = 0.2$ K (cf. SI Fig 1a). Moreover, the temperature in the thermal image (cf. SI Fig 1b) is distributed homogeneously around the IDT without local differences between the three regions.

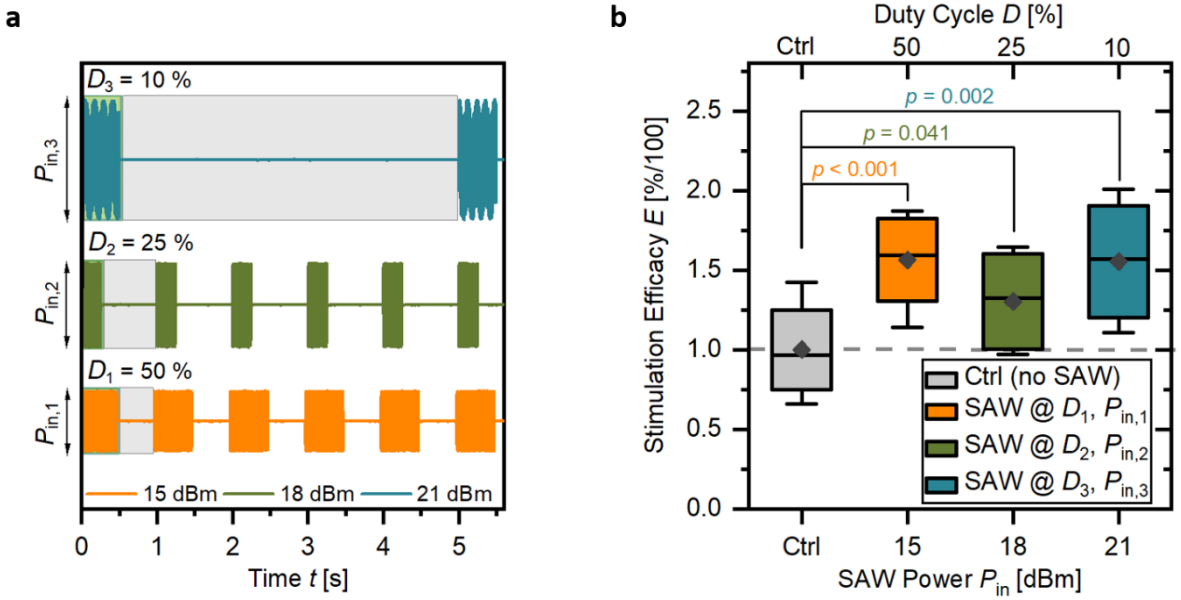

Figure 3 *– Power variation of SAW pulses and the resulting wound healing stimulation efficacy. a) Oscilloscope records of the employed SAW signals at different powers $P_{in,1}$ to $P_{in,3}$ under the condition P_{in}*D ≈ const., b) box plot of the stimulation efficacy of wound healing assays under influence of these SAW signals. Each mean data point consists of N = 6 individual samples; the error bars represent the maximum and minimum value. There were no statistical outliers. The box size represents the standard deviation SD, and the horizontal bar shows the median. A student's independent sample t test yields the significance of the stimulation compared to control samples (N = 11) without SAW treatment at a significance level $\alpha = 0.05$. All SAW parameters induce a significant stimulation effect compared to the control samples.*

According to Eq 5, if the SAW power is doubled (e.g., from P_{in} = 15 dBm to P_{in} = 18 dBm) the duty cycle D must be reduced by half (e.g. from D_1 = 50 % to D_2 = 25 %) to keep $\bar{E}$ constant. This relation is visualized by oscilloscope records in Fig 3a.

We then tested the influence of the different SAW power and duty cycle combinations (i = 1, 2, 3) on wound healing assays under the condition from Eq 5.

The absolute wound healing velocities for (P_i, D_i), following the analyzation scheme in Fig 2, reveal a significant acceleration of wound healing in the aperture regions of SAW-treated samples. The cells in the internal control regions grow at the same speed as the cells in non-treated control samples. However, an interpretation of the absolute velocities is not always ideal, because it does not consider unavoidable variations in cell behavior, chip surface conditions and manual handling between different samples, different chips and different days of experiments that can occur regardless of the experimental protocol's consistency. For the final results shown in Fig 3b, we therefore normalized the absolute data of each sample to its internal control according to Eq 4. The resulting wound healing efficacies are shown in Fig 3b. In total, we analyzed N = 6 samples for each SAW parameter set (P_i, D_i), and additionally N = 11 samples without SAW treatment as external controls. The mean stimulation efficacy of the control samples is $E = 1.00 \mp 0.24$, which was expected because without SAW treatment, there should not be any differences between the wound healing velocities in the aperture and the internal control regions. Interestingly, we obtain higher mean stimulation efficacies for all samples treated with SAW from P_{in} = 15 to 21 dBm. The maximum efficacy $E = 1.56 \mp 0.24$ is reached for P_{in} = 15 dBm, D = 50 %. We performed an independent samples student's t test at a significance level α = 0.05 to test the hypothesis that wound healing in all SAW-treated samples is stimulated compared to the control samples. The normality of the data set was proven previously by a Shapiro Wilk test (SI, Table 2a). All SAW-induced wound healing efficacies exhibit a p value $p < \alpha$, which verifies the significance of the stimulation for all the here employed SAW parameters D and P_{in}. However, we did not detect any significant difference between different parameters (SI, Table 2b). This indicates that the mean energy $\bar{E}_p$ of the SAW signal, rather than the total employed power or duty cycle, is an important condition for the stimulation mechanism.

In the following, we investigate if in addition to the conservation of the mean energy other conditions for successful SAW-stimulated wound healing in our study. Based on the previously found maximum mean stimulation efficacy for the parameter set P_{in} = 15 dBm and D = 50 %, we performed additional experiments under systematic variation of the pulse width τ. For the power variation in Fig 3, we had employed the pulse widths τ_2 = 250 ms and $\tau_{1,3}$ = 500 ms. Here, we test the hypothesis that wound healing stimulation is possible for all pulse widths if the mean energy is still conserved. Exemplary oscilloscope records of the SAW signals with different selected pulse widths are shown in Fig 4a.

Analogous to the power variation experiments, the results of the pulse width variations are summarized by a box plot in Fig 4b. Each mean data point consists of N = 6 samples; the control sample size is N = 13. Normality was tested for this distribution (SI, Table 3a) and we performed a t test under the hypothesis that no stimulation of wound healing is possible for any of the here employed pulse widths τ. For τ < 100 ms, no significant stimulation effect occurs at a significance level α = 0.05 ($p > \alpha$). However, we must reject the hypothesis for $\tau \geq 100$ ms ($p < \alpha$). From a critical pulse width τ_c = 100 ms, we observe a significant stimulation effect with an efficacy of at least E (100 ms) = 1.51 ∓ 0.19. For detailed parameters of the t test results see SI, Table 3b.

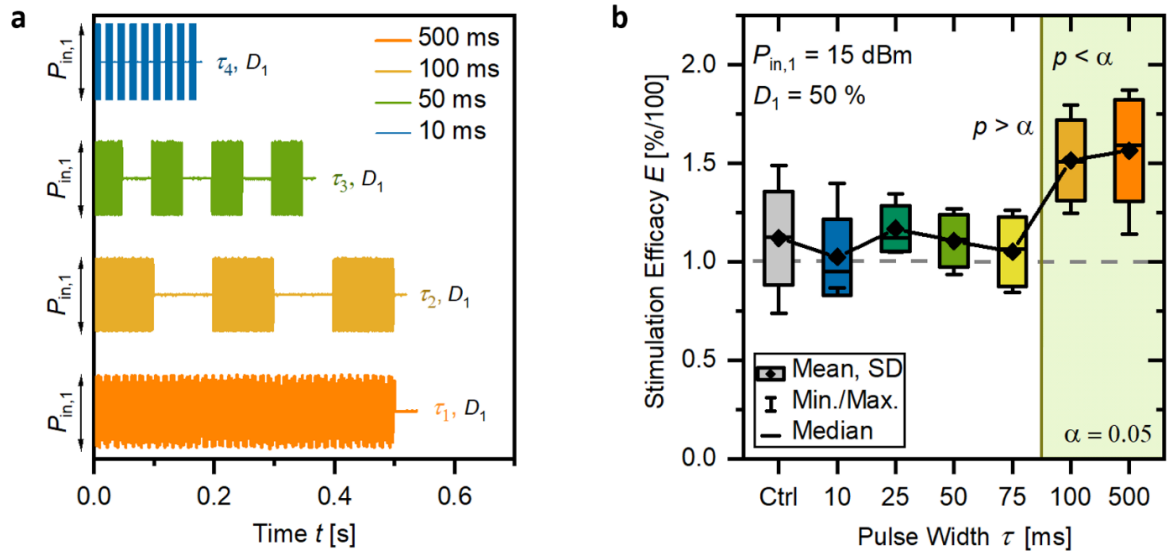

Figure 4 *– Variation of the SAW pulse width τ and the resulting wound healing stimulation efficacy. a) Oscilloscope records of selected SAW signals under variation of the pulse width τ ($P_{in,1}$ = 15 dBm and D_1 = 50 %), b) mean wound healing stimulation efficacies for the pulse width variations: Each mean data point consists of N = 6 samples (control: N = 13). The whiskers of the box plot represent the maximum and minimum efficacies, the box size the standard deviation and the horizontal line the median. A t test shows that only pulse widths above $\tau \geq 100$ ms induce a significant stimulation effect at a significance level $\alpha = 0.05$ compared to the control.*

Although the stimulation efficacy E, which is used as measure for a stimulation effect in this study, is not significant for $\tau < 100$ ms, we observe an interesting behaviour of the absolute wound healing velocities for the pulse width variations (cf. SI, Fig 2c and d): For $\tau < 100$ ms, the absolute velocities can also be significantly enhanced in front of the aperture in comparison to the external control samples. Nevertheless, wound healing is also significantly accelerated in the internal control regions of these samples, which leads to the observed stimulation efficacy of $E \approx 1.0$ in Fig 4b. As mentioned above, deviations between samples that are not related to SAW effects can lead to misinterpretation of the data if the absolute velocities are not normalized to the internal control regions. In this case, however, the absolute data could indicate an additional effect, that could be related to SAW but affects all sample regions, which we will include in our following discussion.

3. DISCUSSION

From the results in Fig 3 and 4, we can derive that SAW stimulation of wound healing assays is limited by the signal's energy and time parameters. These findings complement our knowledge about the limits of SAW parameter sets leading to successful stimulation of wound healing. In previous works, we found that the SAW intensity, and therefore energy, plays an important role for wound healing stimulation with continuous SAW: Brugger et al. tested different powers from P_{in} = 3 dBm up to 21 dBm and found a significant range of stimulation efficacies only for P_{in} = 6, 9 and 12 dBm [13]. This shows that under variation of the total energy, the stimulation effect is not conserved and reaches a maximum in a moderate energy range. The experiments in our study were conducted at a mean energy that is equal to a 12 dBm continuous signal to test if there are other SAW parameter limits to the stimulation effect under optimum conditions. We can conclude that treatments of wound healing assays with continuous signals and signals with long pulse widths (τ = 250 to 500 ms, Fig 3) induce a significant stimulation effect up to E = 201 % (and E = 235 %, respectively, for continuous signals [13]). However, no significant increase in stimulation efficacy is observed for shorter time scales ($\tau < 100$ ms

= τ_c, Fig 4). Still, for these time scales, the absolute wound healing velocities can be enhanced in the whole sample. Consequently, while our underlying high-frequency SAW signal is constant at f_{SAW} = 160 MHz, we here discovered an additional dependency of the cells' behaviour on the overlaying square wave's pulse frequency $f_p = 1/\tau$. From our point of view, this observation could be either directly linked to 1) time scales of the mechanotransduction process in cells as response to mechanical stimuli, like membrane aberrations and calcium mobilization (see section 3.2), or 2) to the viscoelastic properties of the cell layer (see section 3.3), which are especially important for responses of epithelial cells to external mechanical stimuli [25]. However, for the interpretation of mechanic effects, we must first discuss side effects of surface acoustic wave generation like electric fields and acoustic streaming that could contribute to the cells' behaviour (see section 3.1).

3.1 Mechanic vibration as key driver of SAW stimulation

Besides mechanical vibration, the generation of surface acoustic waves induces an electrical field and acoustic streaming. Although electrical fields can also direct cell migration [26], Brugger et al. showed that the electrical field generated by the here used IDT voltage itself does not induce wound healing stimulation [13]. For the stimulation with pulsed signals and therefore pulsed acoustic streaming, microbubbles could play a role. Studies on acoustic tweezing cytometry show that it is possible to measure and mechanically stimulate cells using integrin-anchored microbubbles [27,28]. However, we did not observe any generation of microbubbles in the PH images during live cell imaging, and it is unlikely that bubbles were able to target the necessary sites or number of cells to evoke a stimulation effect as high as observed here. As for the influence of shear forces, the shear stress of the acoustic streaming was quantified in previous reports for the here used SAW chip design and is between $\tau_s \approx 0.1$ - 0.3 dyne/cm^2 [13]. We additionally re-verified the magnitudes of these shear stresses employing particle image velocimetry (PIV) measurements (see SI Fig 2a) and, additionally, tracked the velocity of microbeads in front of the aperture at P_{in} = 15 dBm, D = 50 % over the course of a SAW pulse (SI Fig 2b). According to different reports in literature, a streaming-induced stimulation of wound healing and cell migration was observed for significantly higher shear stress: For $\tau_s > 0.5$ dyne/cm^2, a higher JNK (Jun kinase) and ERK (extracellular signal-regulated kinase) activity in endothelial cells was observed [29]. These proteins belong to the MAP kinases, which play an important role in cell migration [30,31]. Their activation can also lead to an accelerated wound healing of bone stem cells [32]. At even higher shear stress τ_s = 17 dyne/cm^2, Hsu et al. also showed that the migration of cells can be accelerated and is dependent on different streaming patterns of laminar flow which influence focal adhesion dynamics [33]. However, these shear stresses are much higher than the shear stress generated on our SAW chips in the here employed SAW power regime. Obviously, we cannot fully exclude that pulsed shear forces or pulsed electrical fields have the same effect (i.e. no effect) on the cells as continuous forces and fields. But from the fact that we were able to reproduce almost the same stimulation efficacies as in previous works, we deduce that the stimulation mechanism here is most likely the same as in other reports and can be ascribed to the mechanical parts of the SAW.

High-intensity continuous SAW can lead to higher temperatures in a sample. As mentioned above, for the here employed pulsed SAW powers the increase in temperature is very low ($\Delta T \leq 0.2$ K, cf. SI Fig 1). Previous studies already proved that pulsed SAW signals are a useful tool to reduce temperature effects and maintain cell viability while also maintaining the amplitude of the applied wave for cell culture applications [10]. In the context of wound healing stimulation, Brugger et al. showed that SAW treatment of wounds with a continuous P_{in} = 21 dBm signal reduces the proliferation rate and does not induce a stimulation effect compared to moderate SAW powers [13].

3.2 Time scale limits of mechanotransduction processes

Mechanical stimuli can trigger a variety of responses in cells. In their recent review, Ambattu and Yeo proposed intracellular calcium mobilization and the cell membrane as universal key players in the mechanotransduction process of surface acoustic wave stimulation [14]. If the membrane tension is altered by high-frequency mechanical pressure or shear forces generated by acoustic streaming, cells can form vacuoule/vesicle-like dilations (VLDs) to counteract these deformations and activate transmembrane proteins like piezo channels [34]. This can help regulating the transmission of the mechanic force through the cell [35]. As a second messenger, the mechanic compression can drive the influx of Ca^{2+} [36], whereas Ca^{2+} mobilization is dependent on the SAW frequencies and exposure times and can evoke a variety of other signal cascades [14].

Meanwhile, the force transmission in the cell occurs via the cytoskeleton. In this context, actin fibres and the formation and disassembly of focal adhesions play a key role for cell migration [37,38]. However, the formation of focal adhesions occurs over longer time scales than the here employed SAW pulse widths: For example, focal adhesions in protrusive regions of fibroblasts form over the course of minutes [37], so that it is unlikely that, in case of the pulsed SAW signals, the switch between no stimulation and significant stimulation around $\tau_c = 100$ ms is directly caused by these formation mechanisms. However, there are cytoskeletal mechanisms that can occur on shorter time scales: Mazrahi et al. showed that cytoskeleton fluidization, a disruption of the cytoskeleton, and its remodeling, can result from acoustic stimulation with low intensity pulsed ultrasound in human airway smooth muscle (HASM) cells over the course of seconds [39]. The resulting accelerated cytoskeleton re-solidification is known to contribute to healing processes [40]. More detailed studies on the effects of SAW on the cytoskeletal structures are needed to illuminate if this phenomenon also plays a role in SAW-stimulated epithelial wound healing.

All studies on SAW stimulation reviewed by Ambattu and Yeo have relatively long exposure times to the SAW signal in the range of minutes to days [14]. Based on our results, it could be possible that the here mentioned underlying mechanisms of SAW stimulation are only activated by longer exposures to SAW. On the one hand, pulse durations shorter than $\tau_c = 100$ ms may not yet be able to evoke any permanent responses in the cells. This would be a contradiction to Ambattu and Yeo's suggestion that the underlying mechanism of SAW stimulation is independent of the SAW signal's characteristics [14], because our results show a so far unknown limit of signal parameters for dynamically modulated signals with a critical pulse width as lower limit.

On the other hand, it is interesting that the absolute wound healing velocity significantly increases in the whole SAW-treated sample for most pulse widths $\tau < \tau_c$ (SI, Fig 2c and d). In contrast, for $\tau > \tau_c$ only the cells in front of the aperture grow faster compared to non-treated samples. Although the non-treated samples cannot serve as a control for internal characteristics of a sample (like, e.g., differences between the SiO coatings), they still reflect differences in cell behaviour and manual handling between experiments. Therefore, the observed significant increase of the absolute velocities is not necessarily an artifact due to sample deviations but could also be the cause of a SAW-induced effect that is not visible from the normalized data in Fig 4b. This would mean that SAW treatment with lower pulse widths $\tau < \tau_c$ can evoke some sort of secondary stimulation effect in the whole wound. We assume that, in this case, the mechanotransduction or a secondary signalling process from the aperture region must be activated or accelerated, enhancing cell growth in the internal control regions indirectly, where no direct mechanical vibration can affect the cells. To further investigate and prove this assumption, more detailed studies with focus on mechanotransduction and signalling pathways are needed.

3.3 Viscoelastic limits of the cell layer

Since the wavelength of the surface acoustic wave is on the order of magnitude of a whole cell, we think that it is unlikely that the mechanical stimulus targets relatively small structures like focal adhesions or other surface proteins directly. Alternative explanations for the cellular response to SAW stimulation observed in our study, involving more complex mechanotransduction mechanisms, were already discussed in 3.2. We here suggest one other possible aspect related to physical properties of the cells, which is that the stimulation tackles the entire collective layer of migrating cells and its viscoelastic properties. This assumption is supported by previous works on wound healing stimulation, where stimulation effects on non-collectively migrating cells like SaOs-2 cells have been reported, but they were significantly smaller than for collectively migrating MDCK-II cells [11]. The pulse width dependency of the wound healing stimulation (Fig 4b) is a strong indicator that viscoelastic properties of the cell layer might set the limits of the stimulation effect. In literature, the frequency dependency of the elastic and viscous moduli G' and G'' of cells has been demonstrated in multiple studies using methods like optical tweezers, microrheology, magnetic twisting cytometry (MTC) and AFM. For example, Ayala et al. showed in optical tweezers experiments that both G' and G'' of fibroblasts increase in a frequency range between f = 1 to 14 Hz, where the elastic and viscous moduli stay in a range between 10-100 Pa [41]. Fabry et al. (2003) investigated the viscoelastic behaviour of five different cell lines (i.e. epithelial-like F9 and HBE cells) employing MTC, where magnetic beads are directly coupled to the cytoskeleton via integrins [42]. Up to f = 10 Hz, both G' and G'' follow the weak force law (or structural damping equation [43]). However, for f > 10 Hz, G'' exhibits a stronger frequency-dependence and approaches a Newtonian fluid-like behaviour for very high frequencies [42]. Our results from Fig 4 revealed a critical frequency of the square wave for wound healing stimulation of f_c = 10 Hz (τ_c = 100 ms). The comparison with the data from Fabry et al. could confirm that there is a turning point in cellular behaviour around this distinct frequency. If the SAW pulse treatment evokes the same response as MTC, the resulting dominating viscous behaviour of the cells might not be advantageous for migration for square wave frequencies f > 10 Hz (τ < 100 ms). This assumption is supported by the work of Kole et al. (2005), who performed intracellular microrheology experiments on migrating and quiescent fibroblasts [44]. Migrating cells exhibited a higher elasticity of the cytoskeleton than quiescent cells and showed a viscoelastic-liquid behaviour from a frequency limit τ > 200 ms, which is in the same order of magnitude as our critical pulse width. Another interpretation could be that the overall higher absolute wound healing velocities for τ < 100 ms are a result of the frequency dependent viscous properties of cells. For small puls widths, and in turn higher frequencies, the increased viscosity of the confluent cell layer might conveye the stimulus in front of the aperture to the internal control regions.

Many studies point out local differences in cells and suggest that the viscoelastic behaviour is composed of the contribution of the cytoskeleton and of the nuclei. While the cytoskeleton can be treated as a soft-glassy material in the viscoelastic context [45], micropipet aspiration measurements of isolated nuclei showed that nuclei behave more like a viscolastic solid and exhibit three to four times greater elastic moduli G' than intact cells [46]. In this context, Flormann et al. showed that the nucleus and perinucleus of retinal pigmented epithelium cells respond differently to oscillatory microrheology at frequencies from f = 1 to 300 Hz [47]. They indent the cells with an AFM cantilever in the nanometer range and trace back the observed differences to actin bundles in the perinucleus region. Based on these studies, we assume that there are different contributions of nuclei and the cytoskeleton to the SAW stimulation effect, which would be an interesting investigation topic for future studies.

In vivo, cell stimulation becomes even more complex. Transitioning from a 2D wound healing model to cell migration in a 3D matrix, changes in cellular mechanics must be considered. Amongst others, the role of focal adhesion proteins and their modulation of cell motility become more prominent in 3D

models [48]. In vivo, cells additionally do not migrate on solid surfaces, but in an extracellular matrix surrounded by other cells [49]. The application of bulk acoustic waves (BAW) is also a common alternative method to stimulate cells in in vivo systems. Pulsed ultrasound-stimulated wound healing has been proven in animal models: For example, wound healing in female rats was stimulated using low-intensity pulsed ultrasound [6]. Even in human patients, low-intensity pulsed ultrasound can stimulate tibial fracture healing [50], which shows that acoustic stimulation methods can be applied to both in vitro and in vivo systems.

4. CONCLUSION

We here showed that pulsed surface acoustic wave stimulation of MDCK-II cells at high SAW powers can accelerate wound healing up to a stimulation efficacy of E = 201 %. While the stimulation effect is conserved under the condition that the product of the duty cycle D and the SAW power P_{in} (the mean energy) is constant, we did not observe any significant increase of the stimulation efficacy for SAW pulses below a critical pulse width limit $\tau < \tau_c$ with τ_c = 100 ms. By studying these limits of SAW-stimulated wound healing, we hope to contribute to the identification of the underlying mechanisms of the stimulation effect in a phenomenological way. We ascribed the stimulation effect to the mechanical part of the SAW and propose especially the viscoelasticity of the cell layer as the most plausible underlying key mechanism of the here discovered pulse width limit. Time scales of mechanoresponse and mechanotransduction processes like calcium mobilization, the formation of focal adhesions and membrane tension may also play a role. We believe that it is important to reveal further limits like the one found here to further understand the stimulation mechanism and to take them into consideration for possible future medical applications in vivo. Meanwhile, future studies are needed to further illuminate the effects of SAW on intracellular mechanisms like the cytoskeleton, focal adhesions, and other membrane proteins to completely understand and improve wound healing stimulation.

5. MATERIALS AND METHODS

The SAW experiments were performed on $LiNbO_3$ 128° rot XY-cut substrates generating Rayleigh waves via an interdigital transducer (IDT). All chips were produced in the clean room employing photo lithography and the IDT layers were applied using electron beam evaporation. The IDT structure consists of thin gold and titan layers (d(Ti/Au/Ti) = 10/50/10 nm) and an SiO_2 layer ($d(SiO_2)$ = 200 nm) was applied on top of the chip via thermal evaporation to ensure biocompatibility and to protect the electrode structures. The complete experimental setup for SAW-stimulated wound healing assays is visible in Fig 1a. We used culture inserts (Ibidi® GmBH) to create artificial wounds on the chips and a polydimethylsiloxane chamber (Sylgard 184 Silicone Elastomer, Dow Corning) to contain the cell medium (dimensions: $l = b$ = 2.2 cm, wall thickness d = 0.5 cm). The setup was sterilized under UV light for t = 30 min before the experiment. The MDCK-II cells (ECACC Cat.No.: 00062107, Sigma Aldrich) were detached from the culture flask using V = 1 ml Trypsin-EDTA solution (c = 0.25 %, ATCC®), centrifuged at a = 200 g and seeded into the culture inserts at a density of 800000 cells/ml. After t = 20 h of incubation at T = 37 °C and $c(CO_2)$ = 5 %, the culture inserts were removed, the cells were rinsed with PBS (w/o Ca^{2+}, Mg^{2+}, Bio&Sell GmbH) and V = 1 ml fresh culture medium was added (MEM with Earle's Salts and 2.2 g/l $NaHCO_3$, stable glutamine, Bio&Sell GmbH) containing 10 % fetal bovine serum (FBS Superior stabil®, Bio&Sell GmbH) and 1 % Pen/Strep solution (10000 units penicillin, 10 mg streptomycin per ml, Sigma Aldrich®).

We then performed live cell imaging experiments using a phase contrast microscope (Zeiss Axiovert 200 M) with a digital camera (Orca 5G, Hamamatsu) and a stage top CO_2/O_2 incubator (Ibidi® GmbH) at T = 37 °C and $c(CO_2)$ = 5 %. To ensure uniform contrast in the images along the wound, we added anti-evaporation oil (Ibidi® GmbH) to the PDMS chambers on top of the culture medium. Phase contrast scans of the wounds were recorded using a 10x objective over at least t_{WH} = 20 h (Δt_{Scan} = 30 min) until complete wound closure. In all experiments, we measured control samples as well as SAW-treated samples. In the SAW-treated samples, the signal was generated using a frequency generator (SML 01 by Rhode & Schwarz) with an amplifier (Gain = 30 dB; AMP590033H-T; Becker Nachrichtentechnik GmbH) at a resonance frequency of $f_{SAW} \approx 160$ MHz.

The phase contrast scans were binarized using the deep learning algorithm NeuCED (Neural Cell Edge Detector) to determine the stimulation efficacies E of the samples, as visualized by Fig 2a. NeuCED is based on the SegFormer architecture. It consists of (1) the hierarchically structured Transformer encoder module which generates multiscale features and (2) the MLP (multilayer perceptron) decoder which fuses these multi-level features and outputs a 2D segmentation mask. First, a given input image is divided into patches of size 4x4. These patches are then the input to the hierarchical Transformer (Transformer blocks 1-4 in Fig. 2a) encoder to obtain multi-level features at ¼, 1/8, 1/16, 1/32 of the original input image size (Transformer block 1: 1/4, Transfomer block 2: 1/8, Transfomer block 3: 1/16, Transfomer block 4: 1/32). In the decoder phase (named MLP decoder in Fig 2a) the segmentation mask is then predicted out of the multi-level features. For a detailed description of SegFormer and its encoding and decoding see Xie et al. [19].

For the particle image velocimetry (PIV) experiments a Photron high speed camera was used to analyze the flow of 10 µm polystyrene microbeads, as reported earlier [51]. The analysis was performed using a *MATlab* script based on the open source *PIVlab* software by Thielicke [52].

Acknowledgements

C.W. would like to acknowledge support by the Center for NanoScience (CeNS) and funding by the DFG (INST 94/135-1 FUGG, 508235635). K.B. would like to thank the Hanns-Seidel-Stiftung and the "Programm für Chancengleichheit" of the University of Augsburg for financial support. M.L. acknowledges funding by the Bavarian Hightech Agenda within the Munich Quantum Valley doctoral fellowship program. Moreover, we thank Stephan Eberle and Andreas Hörner for technical support.

Data Availability Statement

The data that support the findings of this study are available upon request from the authors.

References

1. Haar G ter: **Therapeutic applications of ultrasound**. *Prog Biophys Mol Biol* 2007, **93**:111–129.

2. Uhlemann C, Heinig B, Wollina U: **Therapeutic Ultrasound in Lower Extremity Wound Management**. *Int J Low Extrem Wounds* 2003, **2**:152–157.

3. Bashardoust Tajali S, Houghton P, MacDermid JC, Grewal R: **Effects of Low-Intensity Pulsed Ultrasound Therapy on Fracture Healing**. *Am J Phys Med Rehabil* 2012, **91**:349–367.

4. Kang J Il, Kim Y-N, Choi H: **Effects of Low-intensity Pulsed Ultrasound and Cryotherapy on Recovery of Joint Function and C-reactive Protein Levels in Patients after Total Knee Replacement Surgery**. *J Phys Ther Sci* 2014, **26**:1033–1036.

5. Driver VR, Yao M, Miller CJ: **Noncontact low-frequency ultrasound therapy in the treatment of chronic wounds: A meta-analysis**. *Wound Repair Regen* 2011, **19**:475–480.

6. Taskan I, Ozyazgan I, Tercan M, Kardas HY, Balkanli S, Saraymen R, Zorlu U, Özügül Y: **A Comparative Study of the Effect of Ultrasound and Electrostimulation on Wound Healing in Rats**. *Plast &amp Reconstr Surg* 1997, **100**:966–972.

7. Yadollahpour A, Mostafa J, Samaneh R, Zohreh R: **Ultrasound Therapy for Wound Healing: A Review of Current Techniques and Mechanisms of Action**. *J Pure Appl Microbiol* 2014, **8**:4071–4085.

8. Baumgartner K, Westerhausen C: **Recent advances of surface acoustic wave-based sensors for noninvasive cell analysis**. *Curr Opin Biotechnol* 2023, **79**:102879.

9. Brugger MS, Grundeen S, Doyle A, Theogarajan L, Wixforth A, Westerhausen C: **Orchestrating cells on a chip: employing surface acoustic waves towards the formation of neural networks**. *Phys Rev E* 2018, **98**:12411.

10. Baumgartner K, Mauritz SCF, Angermann S, Brugger MS, Westerhausen C: **One-dimensional acoustic potential landscapes guide the neurite outgrowth and affect the viability of B35 neuroblastoma cells**. *Phys Biol* 2022, **19**:046005.

11. Stamp MEM, Brugger MS, Wixforth A, Westerhausen C: **Acoustotaxis -in vitro stimulation in a wound healing assay employing surface acoustic waves**. *Biomater Sci* 2016, **4**:1092–1099.

12. Dukes JD, Whitley P, Chalmers AD: **The MDCK variety pack: choosing the right strain**. *BMC Cell Biol* 2011, **12**:43.

13. Brugger MS, Baumgartner K, Mauritz SCF, Gerlach SC, Röder F, Schlosser C, Fluhrer R, Wixforth A, Westerhausen C: **Vibration enhanced cell growth induced by surface acoustic waves as in vitro wound-healing model**. *Proc Natl Acad Sci U S A* 2020, **117**:31603–31613.

14. Ambattu LA, Yeo LY: **Sonomechanobiology: Vibrational stimulation of cells and its therapeutic implications**. *Biophys Rev* 2023, **4**.

15. Ashby WJ, Zijlstra A: **Established and novel methods of interrogating two-dimensional cell migration**. *Integr Biol (United Kingdom)* 2012, **4**:1338–1350.

16. Jonkman JEN, Cathcart JA, Xu F, Bartolini ME, Amon JE, Stevens KM, Colarusso P: **An introduction to the wound healing assay using live-cell microscopy**. *Cell Adh Migr* 2014, **8**:440–451.

17. Campbell C: *Surface Acoustic Wave Devices for Mobile and Wireless Communications, Four Volume Set*. Academic press; 1998.

18. Dransfeld K, Salzman E: **Excitation, Detection, and Attenuation of High-Frequency Elastic Surface Waves**. *Phys Acoust Princ Methods* 2012, **7**:219–271.

19. Xie E, Wang W, Yu Z, Anandkumar A, Alvarez JM, Luo P: **SegFormer: Simple and Efficient Design for Semantic Segmentation with Transformers**. *Adv Neural Inf Process Syst* 2021, **15**:12077–12090.

20. Dosovitskiy A, Beyer L, Kolesnikov A, Weissenborn D, Zhai X, Unterthiner T, Dehghani M, Minderer M, Heigold G, Gelly S, et al.: **an Image Is Worth 16X16 Words: Transformers for Image Recognition At Scale**. *ICLR 2021 - 9th Int Conf Learn Represent* 2021,

21. Zheng S, Lu J, Zhao H, Zhu X, Luo Z, Wang Y, Fu Y, Feng J, Xiang T, Torr PHS, et al.: **Rethinking Semantic Segmentation from a Sequence-to-Sequence Perspective with Transformers**. *Proc IEEE Comput Soc Conf Comput Vis Pattern Recognit* 2021, doi:10.1109/CVPR46437.2021.00681.

22. Wang W, Xie E, Li X, Fan D-P, Song K, Liang D, Lu T, Luo P, Shao L: **Pyramid Vision Transformer: A Versatile Backbone for Dense Prediction without Convolutions**. *2021 IEEE/CVF Int Conf Comput Vis* 2021,

23. Liu Z, Lin Y, Cao Y, Hu H, Wei Y, Zhang Z, Lin S, Guo B: **Swin Transformer**. *2021 IEEE/CVF Int Conf Comput Vis* 2021,

24. Chu X, Tian Z, Wang Y, Zhang B, Ren H, Wei X, Xia H, Shen C: **Twins: Revisiting the Design of Spatial Attention in Vision Transformers**. *Adv Neural Inf Process Syst* 2021, **12**:9355–9366.

25. Janshoff A: **Viscoelastic properties of epithelial cells**. *Biochem Soc Trans* 2021, **49**:2687–2695.

26. Tai G, Reid B, Cao L, Zhao M: **Electrotaxis and Wound Healing: Experimental Methods to Study Electric Fields as a Directional Signal for Cell Migration**. In *Methods in Molecular Biology*. . 2009:77–97.

27. Chen D, Sun Y, Gudur MSR, Hsiao Y-S, Wu Z, Fu J, Deng CX: **Two-Bubble Acoustic Tweezing Cytometry for Biomechanical Probing and Stimulation of Cells**. *Biophys J* 2015, **108**:32–42.

28. Yang C, Chen D, Hong X: **Estimation of viscoelastic properties of cells using acoustic tweezing cytometry**. *J Ultrasound Med* 2016, **35**:2537–2542.

29. Jo H, Sipos K, Go YM, Law R, Rong J, McDonald JM: **Differential effect of shear stress on extracellular signal-regulated kinase and N-terminal jun kinase in endothelial cells: G(i)2- and Gβ/γ- dependent signaling pathways**. *J Biol Chem* 1997, **272**:1395–1401.

30. Huang C, Jacobson K, Schaller MD: **MAP kinases and cell migration**. *J Cell Sci* 2004, **117**:4619–4628.

31. Tanimura S, Takeda K: **ERK signalling as a regulator of cell motility**. *J Biochem* 2017, **162**:145–154.

32. Zhang M, Sun L, Wang X, Chen S, Kong Y, Liu N, Chen Y, Jia Q, Zhang L, Zhang L: **Activin B promotes BMSC-mediated cutaneous wound healing by regulating cell migration via the JNK-ERK signaling pathway**. *Cell Transplant* 2014, **23**:1061–1073.

33. Hsu P-P, Li S, Li Y-S, Usami S, Ratcliffe A, Wang X, Chien S: **Effects of flow patterns on endothelial cell migration into a zone of mechanical denudation**. *Biochem Biophys Res Commun* 2001, **285**:751–759.

34. Lewis AH, Grandl J: **Mechanical sensitivity of Piezo1 ion channels can be tuned by cellular membrane tension**. *Elife* 2015, **4**.

35. Wang J, Jiang J, Yang X, Zhou G, Wang L, Xiao B: **Tethering Piezo channels to the actin cytoskeleton for mechanogating via the cadherin-β-catenin mechanotransduction complex**. *Cell Rep* 2022, **38**:110342.

36. Roberts SR, Knight MM, Lee DA, Bader DL: **Mechanical compression influences intracellular Ca 2+ signaling in chondrocytes seeded in agarose constructs**. *J Appl Physiol* 2001, **90**:1385–1391.

37. Webb DJ, Donais K, Whitmore LA, Thomas SM, Turner CE, Parsons JT, Horwitz AF: **FAK-Src signalling through paxillin, ERK and MLCK regulates adhesion disassembly**. *Nat Cell Biol* 2004, **6**:154–161.

38. Zhao X, Guan J-L: **Focal adhesion kinase and its signaling pathways in cell migration and angiogenesis**. *Adv Drug Deliv Rev* 2011, **63**:610–615.

39. Mizrahi N, Zhou EH, Lenormand G, Krishnan R, Weihs D, Butler JP, Weitz DA, Fredberg JJ, Kimmel E: **Low intensity ultrasound perturbs cytoskeleton dynamics**. *Soft Matter* 2012, **8**:2438.

40. Hu Y, Wan JMF, Yu ACH: **Cytomechanical Perturbations during Low-Intensity Ultrasound Pulsing**. *Ultrasound Med Biol* 2014, **40**:1587–1598.

41. Ayala YA, Pontes B, Ether DS, Pires LB, Araujo GR, Frases S, Romão LF, Farina M, Moura-Neto V, Viana NB, et al.: **Rheological properties of cells measured by optical tweezers**. *BMC Biophys* 2016, **9**:1–11.

42. Fabry B, Maksym GN, Butler JP, Glogauer M, Navajas D, Taback NA, Millet EJ, Fredberg JJ: **Time scale and other invariants of integrative mechanical behavior in living cells**. *Phys Rev E - Stat Physics, Plasmas, Fluids, Relat Interdiscip Top* 2003, **68**:1–18.

43. Fredberg JJ, Stamenovic D: **On the imperfect elasticity of lung tissue**. *J Appl Physiol* 1989, **67**:2408–2419.

44. Kole TP, Tseng Y, Jiang I, Katz JL, Wirtz D: **Intracellular Mechanics of Migrating Fibroblasts**. *Mol Biol Cell* 2005, **16**:328–338.

45. Sollich P: **Rheological constitutive equation for a model of soft glassy materials**. *Phys Rev E - Stat Physics, Plasmas, Fluids, Relat Interdiscip Top* 1998, **58**:738–759.

46. Guilak F, Tedrow JR, Burgkart R: **Viscoelastic Properties of the Cell Nucleus**. *Biochem Biophys Res Commun* 2000, **269**:781–786.

47. Flormann DAD, Anton C, Pohland MO, Bautz Y, Kaub K, Terriac E, Schäffer TE, Rheinlaender J, Janshoff A, Ott A, et al.: **Oscillatory Microrheology, Creep Compliance and Stress Relaxation of Biological Cells Reveal Strong Correlations as Probed by Atomic Force Microscopy**. *Front Phys* 2021, **9**:1–12.

48. Fraley SI, Feng Y, Krishnamurthy R, Kim D-H, Celedon A, Longmore GD, Wirtz D: **A distinctive role for focal adhesion proteins in three-dimensional cell motility**. *Nat Cell Biol* 2010, **12**:598–604.

49. Stamm A, Reimers K, Strauß S, Vogt P, Scheper T, Pepelanova I: **In vitro wound healing assays – state of the art**. *BioNanoMaterials* 2016, **17**:79–87.

50. Heckman J, Ryaby J, McCabe J, Frey J, Kilcoyne R: **Acceleration of tibial fracture-healing by non-invasive, low-intensity pulsed ultrasound**. *J Bone Jt Surg* 1994, **76**:26–34.

51. Strobl FG, Breyer D, Link P, Torrano AA, Bräuchle C, Schneider MF, Wixforth A: **A surface acoustic wave-driven micropump for particle uptake investigation under physiological flow conditions in very small volumes**. *Beilstein J Nanotechnol* 2015, **6**:414–419.

52. Thielicke W, Stamhuis EJ: **PIVlab – Towards User-friendly, Affordable and Accurate Digital Particle Image Velocimetry in MATLAB**. *J Open Res Softw* 2014, **2**.